

Experimental validation of plasma tomography algorithms at ISTTOK

D. Hachmeister, D. R. Ferreira, D. D. Carvalho, R. V. Cardoso, H. Alves, H. Figueiredo and H. Fernandes

*Instituto de Plasmas e Fusão Nuclear, Instituto Superior Técnico, Universidade de Lisboa
1049-001 Lisboa, Portugal*

E-mail: daniel.hachmeister@tecnico.ulisboa.pt

ABSTRACT: Plasma tomography is an ill-conditioned inversion problem. Algorithms based on Tikhonov regularization and minimum Fisher information try to overcome this issue by introducing regularization parameters that require empirical tuning. In general, to validate the implementation of these algorithms, either artificial phantoms are used, or one must rely on information provided by other diagnostics. In this work, an experimental setup was developed that allows the use of physical phantoms to tune and validate the reconstruction algorithms. The setup was assembled in a replica of the ISTTOK tokamak with a cylindrical cold cathode lamp placed perpendicular to the poloidal plane at multiple radial and angular positions. It is assumed that this physical phantom acts approximately as a point source in the emissivity profile. Knowing these profiles *a priori*, it is possible to compare them with the reconstructions produced by the algorithms, in order to tune and optimize the reconstruction parameters. After validation with these physical phantoms, several reconstructions were successfully computed for some tokamak discharges.

KEYWORDS: Plasma Tomography; Regularization; Beam-Width Effects

1 Introduction

Plasma tomography is a technique used to reconstruct the spacial distribution of a cross-sectional plasma profile from its line integrated measurements [1]. Here we focus on the plasma radiation profile which is reconstructed from plasma emissivity measurements. The reconstructed images (or tomograms) are obtained by sampling the plasma along lines of sight with arrays of optical sensors, such as pinhole cameras. One way of stating the tomography problem is with the matrix equation:

$$\mathbf{f} = \mathbf{T} \cdot \mathbf{g} \quad (1.1)$$

where \mathbf{f} represents the set of measurements from the various sensors, \mathbf{g} is the emissivity function represented on some orthogonal basis, usually a rectangular pixel grid, and \mathbf{T} is the so-called geometry matrix that describes how a given point in the emissivity profile \mathbf{g} contributes to the measurement of each sensor in \mathbf{f} .

The problem is ill-conditioned in nature, and to circumvent this problem some sort of regularization is needed. A common approach is to require smoothness of the reconstructed profile. The solution can be found by minimizing [2]:

$$\phi = \|\mathbf{T} \cdot \mathbf{g} - \mathbf{f}\|^2 + \lambda \|\mathbf{g}^T \cdot \mathbf{H} \cdot \mathbf{g}\|^2 \quad (1.2)$$

where the first term is the typical least-squares minimization (χ^2) and the second is the regularization term. Matrix \mathbf{H} represents the type of regularization to be imposed and λ is the regularization parameter, used to tune the strength of such regularization.

The correct implementation of a tomography algorithm depends on an accurate representation of the geometry matrix \mathbf{T} . The simplest implementation is based on a line-of-sight approach (LoS). The LoS matrix assumes that the pixels of the tomogram that contribute to the measurement of a given sensor lie along a straight line. This approximation is well motivated by the conservation of étendue [3]. However, a more complete description needs to take into account the full geometry of the pinhole and the sensors, which yields a volume of sight approach (VoS) [4].

Studies have been conducted to determine performance of both the LoS and the VoS methods in a simulated environment, concluding that the VoS approach is recommended [4]. However, there is still a lack of experimental evidence. In this work, we use an experimental setup to compare both methods.

2 Experimental Setup

The ISTTOK tokamak has a circular cross-section with a major radius of 46 cm and a minor radius of 8.5 cm at the limiter. The tomography diagnostic used in this work consists of two pinhole cameras toroidally aligned and positioned at poloidal angles 0° and 90° . Each camera contains a linear array of 16 photodiodes behind the pinhole, defining the lines of sight for each sensor. Figure 1 shows the cameras and the lines of sight. The photodiodes (AXUV20ELG by Opto Diode) have a spectral range from soft X-rays to infrared.¹ No optical filtering is used.

¹The photodiode array AXUV20ELG has 20 diodes of which we only use the middle 16 due to hardware constraints and limitations in the acquisition system.

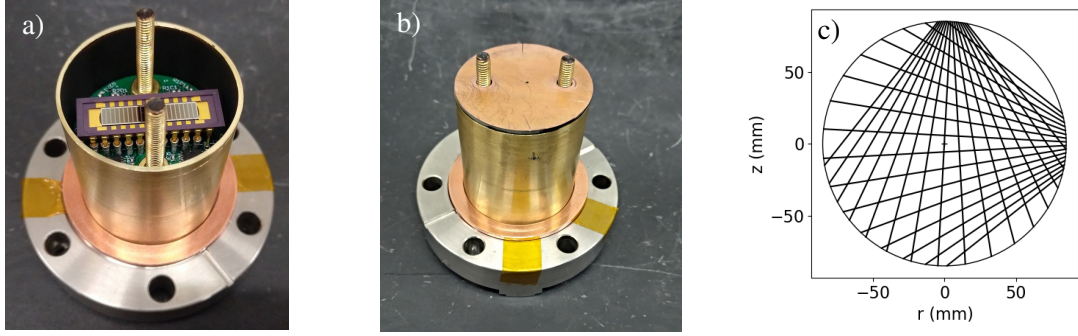


Figure 1. a) Camera without the pinhole lid to show the photodiode array; b) Camera with the pinhole lid; c) lines of sight for the cameras positioned at 0° and 90°.

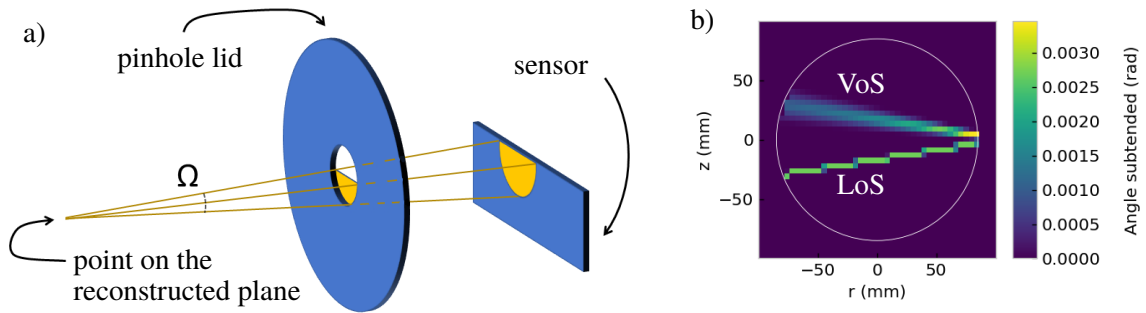


Figure 2. a) Example of the solid angle subtended by a pinhole setup; b) Individual pixel contributions to the measurement of a given sensor in both the VoS (top) and LoS (bottom) approximations.

The geometry matrix (VoS) for this setup can be computed using ray-tracing libraries [4] or by explicit calculation of the solid angle [5], which is the approach we use here. Figure 2(a) shows the solid angle Ω that needs to be computed at each point in space. This calculation assigns a certain weight to each pixel on the image plane proportional to Ω . In figure 2(b) we plot the values of the solid angle for each pixel. These values form a fading cone from the sensor. The LoS is also plotted for comparison, for a similar view with the same solid angle.

In order to compare both approaches, a movable light source was used. The light source consisted of a cylindrical cold cathode lamp with a length of 50 mm and a diameter of 4 mm. The lamp was held by a plastic structure inside a replica of the tokamak vessel, as shown in Figure 3(a). This structure allowed the placement of the source at different radial and angular positions. The lamp has an expected point-like emissivity for pixel sizes larger than its diameter. Knowing the expected emissivity profile, we can then evaluate the quality of the reconstructions performed by the algorithm. The algorithm used in this work was the minimum Fisher information [2].

The pixel size used in this work was chosen to be the diameter of the lamp (around 4mm). At this resolution the lamp is expected to act as a point source. The chosen pixel size also needed to allow a clear distinction between the VoS and LoS matrices. This translates into having more than one pixel width for the volume of sight. In our case, the volumes of sight are three pixels wide.

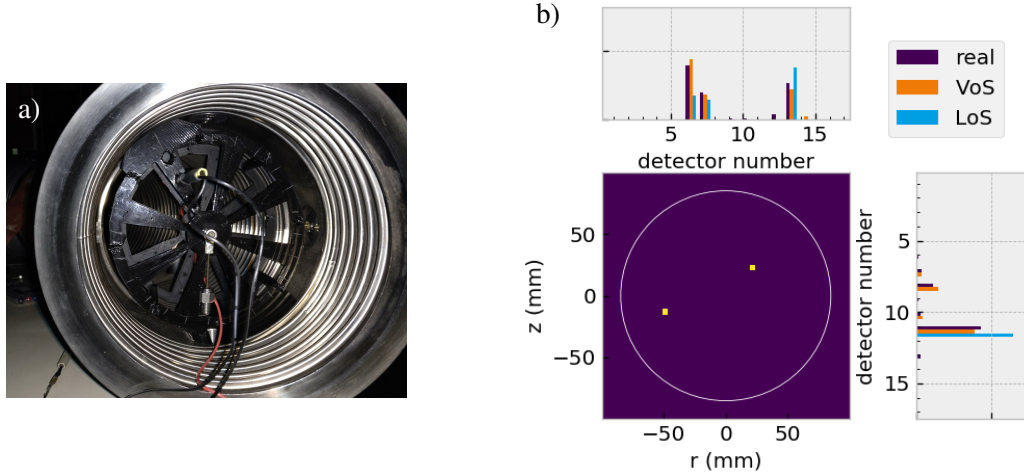


Figure 3. a) Cold cathode lamp and supporting structure inside the vessel replica; b) real vs. expected signals from the VoS and LoS geometries.

3 Results

Given the expected emissivity \mathbf{g} of the lamp, we applied matrix \mathbf{T} to get the expected signals for the LoS and the VoS approaches. We then compared these results to the actual signals obtained from experiment. Figure 3(b) shows an example of the real data versus the data predicted by the two \mathbf{T} matrices for two different lamp positions. The mean squared difference between expected and measured signals was 70% larger in the LoS case compared to the VoS case, evidence that the VoS matrix is indeed a more accurate representation of the setup geometry.

Reconstructions were performed with the acquired signals to determine the influence of each geometry matrix on the quality of the reconstructed profiles. To evaluate the resemblance between the reconstructed profile and the expected point-like emissivity, we computed the structural similarity index (SSIM) [6] between them. The VoS approach performed better in 50% of the cases, while the LoS performed better on 25% of the cases. The remaining 25% of the cases correspond to an equal performance of both methods.

The better performance of the LoS approach was observed in instances where the lamp was aligned with a single sensor in each camera. In these cases, the algorithm yielded a sharp emissivity profile, which scored better than the somewhat more diffuse solution provided by the VoS approximation. This is probably due to the larger area of the volumes of sight compared to the lines of sight.

Figures 4(a & b) show the reconstructions from an experiment with single sensor illumination. It is apparent that the LoS approach leads to a better reconstruction in the sense that it is closer to a point-like source. On the other hand, figures 4(c & d) show the results of multiple-sensor illumination. In this case, the LoS yields a broader profile because consecutive lines are further apart than consecutive volumes. In our case, consecutive volumes have actually a small overlap.

Finally, we compared both matrices by reconstructing a tomogram for a real shot.² Figure 5 shows the results of the reconstruction with both the VoS and LoS matrices. Both reconstructions

²Shot #45988 @309ms. Electron temperature at the core and electron density are respectively 150 eV and $3 \times 10^{18} \text{m}^{-3}$.

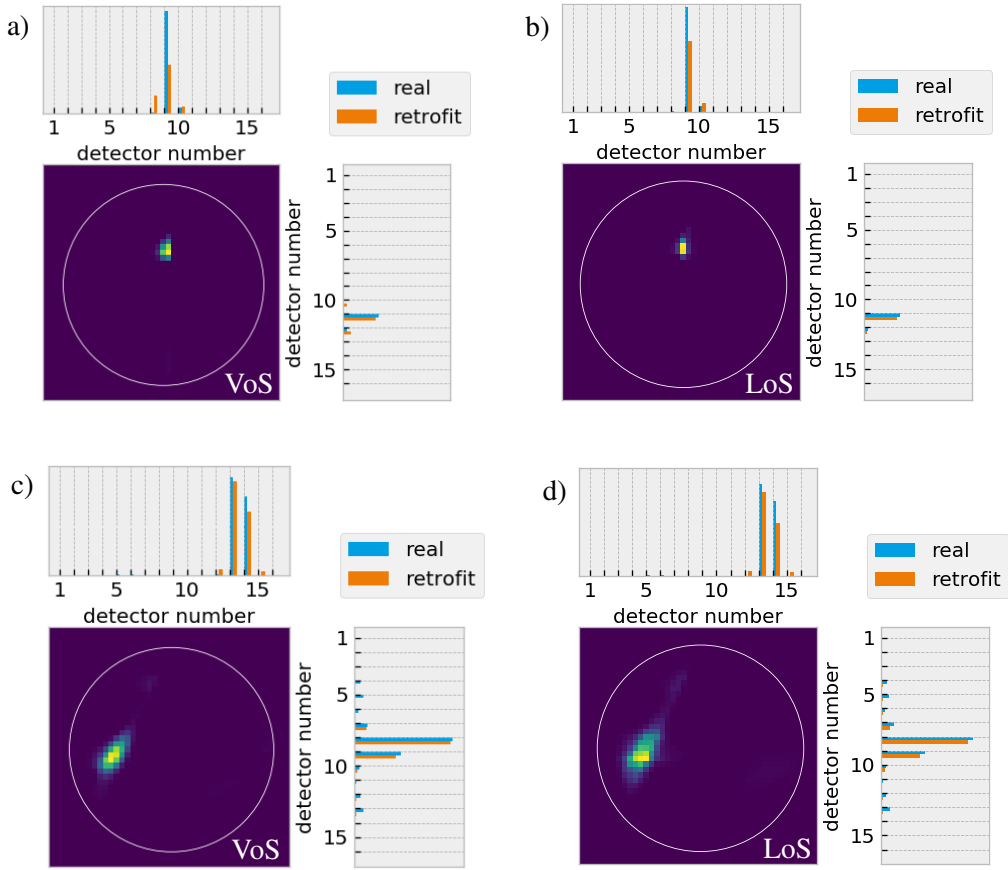


Figure 4. Single sensor illumination a) & b) vs. multiple sensor illumination c) & d) for the LoS and the VoS approximations. Histograms show, for each camera, the signals measured by the detectors and the retrofit signals computed with eq. (1.1).

were done with the same regularization constant λ . The LoS tomogram appears to be less smooth than the VoS one. In fact, referring to equation (1.2) the VoS tomogram has a regularization term $\|\mathbf{g}^T \cdot \mathbf{H} \cdot \mathbf{g}\|^2$ that is 25 times smaller than the same term in the LoS case, indicating that it is in fact more smooth. Meanwhile, both reconstructions have a similar χ^2 , with only a 15% difference. This suggests that there is an intrinsic regularization inherent to matrix \mathbf{T} in the VoS case, as would be expected by the broader nature of the volumes of sight.

4 Conclusion

The volume of sight (VoS) approach performed better than the line of sight (LoS) approach in most of our experiments. Although a point source does not resemble an actual plasma, if a point source can be accurately reconstructed then there might be a better chance of detecting sharp features over the plasma background such as blob filaments. For this reason, we recommend the use of the VoS approach.

The experimental setup used in this work proved to be a valuable tool to calibrate the optical system of ISTTOK and to compare the LoS and the VoS approaches. It can be used in the future to

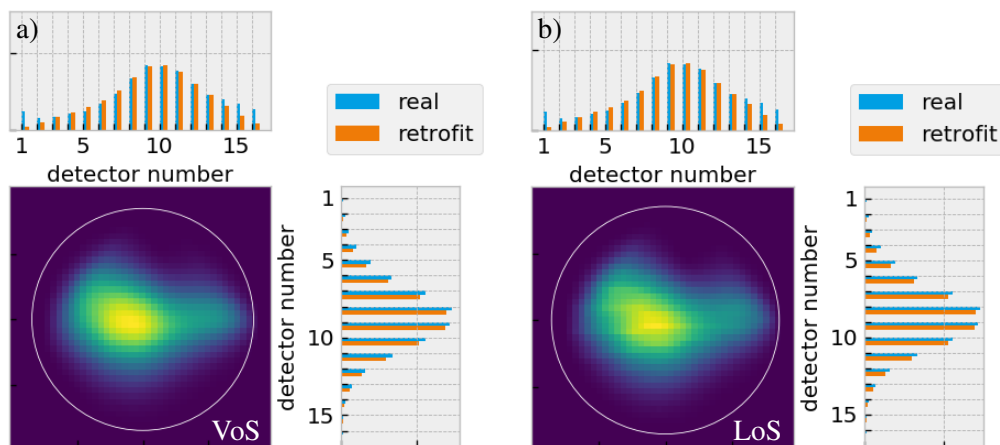


Figure 5. Plasma reconstructions made with a) volume of sight matrix and b) line of sight matrix. Histograms show, for each camera, the signals measured by the detectors and the retrofit signals computed with eq. (1.1).

compare the performance of other tomography algorithms.

Finally, it is worth mentioning that the sparsity of the geometry matrix changed from 2% in the LoS case to 10% in the VoS case. Implementations that rely on sparse matrix calculations may therefore see their computation time affected. Since our implementation did not use sparse calculations, we observed no difference in computation time.

Acknowledgments

IPFN activities received financial support from *Fundação para a Ciência e Tecnologia* through project UID/FIS/50010/2019.

References

- [1] J. Mlynar, T. Craciunescu, D. R. Ferreira, P. Carvalho, O. Ficker, O. Grover et al., *Current Research into Applications of Tomography for Fusion Diagnostics*, *Journal of Fusion Energy* **38** (8, 2018) 458–466.
- [2] J. Mlynar, M. Imrisek, V. Weinzettl, M. Odstrcil, J. Havlicek, F. Janky et al., *Introducing minimum Fisher regularisation tomography to AXUV and soft x-ray diagnostic systems of the COMPASS tokamak*, *Review of Scientific Instruments* **83** (10, 2012) 10E531.
- [3] M. Anton, H. Weisen, M. J. Dutch, W. v. d. Linden, F. Buhlmann, R. Chavan et al., *X-ray tomography on the TCV tokamak*, *Plasma Physics and Controlled Fusion* **38** (11, 1996) 1849–1878.
- [4] M. Carr, A. Meakins, M. Bernert, P. David, C. Giroud, J. Harrison et al., *Description of complex viewing geometries of fusion tomography diagnostics by ray-tracing*, *Review of Scientific Instruments* **89** (8, 2018) 083506.
- [5] D. Vezinet, V. Igochine, M. Weiland, Q. Yu, A. Gude, D. Meshcheriakov et al., *Non-monotonic growth rates of sawtooth precursors evidenced with a new method on ASDEX Upgrade*, *Nuclear Fusion* **56** (8, 2016) 086001.
- [6] Z. Wang, A. Bovik, H. Sheikh and E. Simoncelli, *Image Quality Assessment: From Error Visibility to Structural Similarity*, *IEEE Transactions on Image Processing* **13** (4, 2004) 600–612.